RSC Advances

PAPER

View Article Online
View Journal | View Issue



Cite this: *RSC Adv.*, 2020, **10**, 41577

# Makerspace microfabrication of a stainless steel 3D microneedle electrode array (3D MEA) on a glass substrate for simultaneous optical and electrical probing of electrogenic cells

Paola M. Morales-Carvajal, †[a] Avra Kundu, †[a] Charles M. Didier, [ab] Cacie Hart, [ac] Frank Sommerhage [a] and Swaminathan Rajaraman*[abcd]

Microfabrication and assembly of a Three-Dimensional Microneedle Electrode Array (3D MEA) based on a glass-stainless steel platform is demonstrated involving the utilization of non-traditional "Makerspace Microfabrication" techniques featuring cost-effective, rapid fabrication and an assorted biocompatible material palette. The stainless steel microneedle electrode array was realized by planar laser micromachining and out-of-plane transitioning to have a 3D configuration with perpendicular transition angles. The 3D MEA chip is bonded onto a glass die with metal traces routed to the periphery of the chip for electrical interfacing. Confined precision drop casting (CPDC) of PDMS is used to define an insulation layer and realize the 3D microelectrodes. The use of glass as a substrate offers optical clarity allowing for simultaneous optical and electrical probing of electrogenic cells. Additionally, an interconnect using 3D printing and conductive ink casting has been developed which allows metal traces on the glass chip to be transitioned to the bottomside of the device for interfacing with commercial data acquisition/analysis equipment. The 3D MEAs demonstrate an average impedance/phase of ~13.3 kΩ/−12.1° at 1 kHz respectively, and an average 4.2 μV noise. Lastly, electrophysiological activity from an immortal cardiomyocyte cell line was recorded using the 3D MEA demonstrating end to end device development.

Received 11th July 2020
Accepted 6th October 2020

DOI: 10.1039/d0ra06070d

rsc.li/rsc-advances



## 1. Introduction

Cells have a membrane potential that is the basis for integrating, generating, driving and transmitting signals from the cells to the external environment.[1] Changes in ionic permeability translate into the electrical activity that regulates cellular physiology. Phenomena such as the potential from cardiac action, neurotransmission and production of neurotransmitters, cell proliferation, activation and differentiation, ion transport and the release of hormones are all based on electrical activity.[2] Cellular electrophysiology is the study of the electrical properties of biological cells and tissues and the interpretation of this activity.[3,4] Microelectrode arrays are one of the primary interfaces used to record and stimulate electrical activity from the *in vitro* electrogenic cell cultures and serve as label-free platforms in the pharmaceutical industry to provide information for instance about a drug's efficacy.[5] Microelectrode arrays have become vital in different fields such as pharmacology, toxicology, high throughput screening, stem cell differentiation *etc.* to obtain *in vitro* electrical measurements of different clusters of neurons, cells, tissues, *etc.*[6] Microelectrode arrays are increasingly being used for "disease-on-a-chip" models for neural diseases such as Parkinson's, epilepsy, Amyotrophic Lateral Sclerosis (ALS), neuropathic pain, and autism spectrum disorders.[5] MEAs can therefore perform clinically relevant nerve conduction tests and measure changes in electrophysiological properties that reflect the effects on the human nervous system.

Microelectrode arrays are additionally used in cardiac applications, for instance in cardiac cell therapeutics or to improve the existing cardiac safety mechanisms.[7] Microelectrode arrays serve as a platform to evaluate arrhythmia risk and such studies are vital to understanding the complex and varied nature of arrhythmia.[8] Microelectrode array technology plays an important role in advancing human health by pushing the boundaries of disease modeling and therapeutics including drug discovery along with safety and toxicology studies. Conventional microelectrode arrays are planar (2D) in nature and typically fabricated in state of the art cleanroom facilities.[7,9]

[a]*NanoScience Technology Center (NSTC), University of Central Florida, 4353 Scorpius Street, Orlando, FL 32816-0120, USA. E-mail: swaminathan.rajaraman@ucf.edu; Tel: +1-407-823-4339*

[b]*Burnett School of Biomedical Sciences, University of Central Florida, Orlando, FL 32827, USA*

[c]*Department of Materials Science & Engineering, University of Central Florida, Orlando, FL 32826, USA*

[d]*Department of Electrical & Computer Engineering, University of Central Florida, Orlando, FL 32826, USA*

† Contributed equally to the paper.

In order to better mimic *in vivo*-like conditions[10,11] for *in vitro* applications, 3D cell culture models are becoming increasingly popular as they are better able to capture signaling pathways and drug responsiveness in disease states when compared to 2D models.[12–15] 3D cell cultures enable the formation of dynamic and spatial gradients of soluble factors that influence cellular migration, better represent cell to cell communication and differentiation to accurately predict *in vivo* tissue functions and drug response signatures.[15,16] This has led to an increasing need to extend cell culture matrices and support scaffolds to the third dimension.[11] Such culture models would help realize "disease-on-a-plate" and fully functional "organ-on-a-chip" models to promote cell/tissue growth and regeneration *in vitro*.[17]

In response to the growth of 3D cellular models specifically for electrogenic cells, there has been a growing need to extend *in vitro* microelectrodes to the third dimension. Three-Dimensional Microneedle Electrode Array (3D MEAs) would allow for simple, high throughput screening and measurement of network dynamics for the study of 3D microengineered cellular systems including but not limited to central or peripheral nervous system applications such as the recently developed Human Nerve-on-a-Chip (HNoaC) system which is 3D in nature and can be used for evaluating electrophysiological and histological metrics[18] and other organ systems for instance extracellular microelectrode recordings from cardiac myocytes towards *in vitro* heart-on-a-chip models.[19] Enabling 3D functionality in MEAs built atop optically transparent materials would enable simultaneous extraction of optical and electrical data from 3D cell cultures.

Microfabrication of 3D MEAs using conventional cleanroom-based techniques is particularly challenging because most of the techniques are suited for two-dimensional device processing. These techniques have been adopted to realize the earliest interfaces created on silicon wafers and glass coverslips.[20,21] Several polymers such as polydimethylsiloxane, parylene *etc.*, have emerged as a newer material set for MEA fabrication providing several advantages over traditional glass/silicon substrates. They not only offer simpler microfabrication methods but also provide physical flexibility, proven biocompatibility and biostability.[22,23] Additionally, backend technologies such as Printed Circuit Boards (PCBs), Chip On Board (COB), and flip chip technologies have been utilized to interface the microfabricated devices with commercial amplification systems for data processing, analysis and plotting.[5] Recently, 3D printing of photopolymeric resins have been reported to realize MEAs having electrode densities up to a commercially popular 8 × 8 array allowing for the MEAs to be "used and tossed" and moving the manufacturing from the cleanroom to makerspaces.[24] The use of makerspace techniques compares very favorably with traditional glass MEAs in terms of design to device while representing a dramatic reduction in cost, timeline for fabrication, reduction in the number of steps and the need for sophisticated microfabrication and packaging equipment along with the capability of monolithic microfabrication of the device and package for seamless integration with commercial data acquisition and amplification systems.[24]

In this paper, the microfabrication and packaging of a stainless steel (SS) 3D MEA assembled on a glass substrate is reported. The device fabrication employs non-traditional "Makerspace Microfabrication"[11,24,25] techniques to realize the device predominantly outside the cleanroom. The use of "Makerspace Microfabrication" has been demonstrated previously by the authors to realize a 2D MEA up to a commercially popular 8 × 8 array as stated earlier.[24] The present work differs from the earlier reported method on several fronts. First, we use different toolbox technologies present in the makerspace environment to realize microneedle electrodes in 3D instead of 2D electrodes as reported in our prior work. While the prior work relied heavily on 3D printing to fabricate the 2D MEA, this work only relies on 3D printing for realizing a custom jig for interfacing the device with commercially available data acquisition systems. Second, the substrate presented as a part of this work is glass; a completely transparent platform suitable for the optical interrogation (upright, confocal or inverted microscopy) of the cell culture. Third, the use of the glass platform allows for the use of proven biocompatible materials like such as stainless steel, titanium, gold, polydimethylsiloxane (PDMS), polyethylene terephthalate glycol (PET-G) to facilitate cytocompatibilty with cardiac and other cell lines. Lastly, we report electrophysiological testing in this paper. Specifically, laser micromachining is used to ablate a SS sheet with ten (10) obelisk-type microneedle geometries. Eight (8) obelisks are arranged in a linear array and the construct is terminated by two (2) obelisks adjacent to one another. The dimensions of the obelisk ablation are designed to incorporate a height of 400 μm and a width of 300 μm once it is transitioned out-of-plane to have a 3D configuration. The pitch of the obelisk is 600 μm in the linear portion of the array. The tip of the obelisk geometry can additionally penetrate into prepared slices from brain and other electrogenic tissues.[26] The 3D obelisk array is subsequently assembled on a highly transparent glass chip with metallized titanium–gold (Ti–Au) traces making the platform capable of simultaneous optical and electrical probing. The array of electrodes is isolated from each other by laser micromachining to have ten (10) individual recording/stimulation sites. Controlled precision drop-casting (CPDC) is used to define the PDMS insulation material after affixing the PET-G culture well onto the glass chip. Cellular electrophysiological activity of HL-1 cells, a cardiac muscle cell line from the AT-1 mouse was measured after approximately 2 days *in vitro* (DIV).

## 2. Materials and methods

### 2.1 Microfabrication of three-dimensional stainless steel microneedle electrode array (3D MEA)

The obelisk shaped MEA was designed using SolidWorks, Dassault Systems Inc., (Velizy-Villacoublay, France) in Drawing Interchange format (*.dxf). The length of the construct was 4200 μm with a width 500 μm terminating with a circular region having a diameter of 800 μm. MEA consisting of ten (10) electrodes were placed inside the described silhouette and a single planar microneedle cutout had a base width of 300 μm, length of 400 μm and a pitch of 600 μm. Fig. 1(a) shows the schematic

 

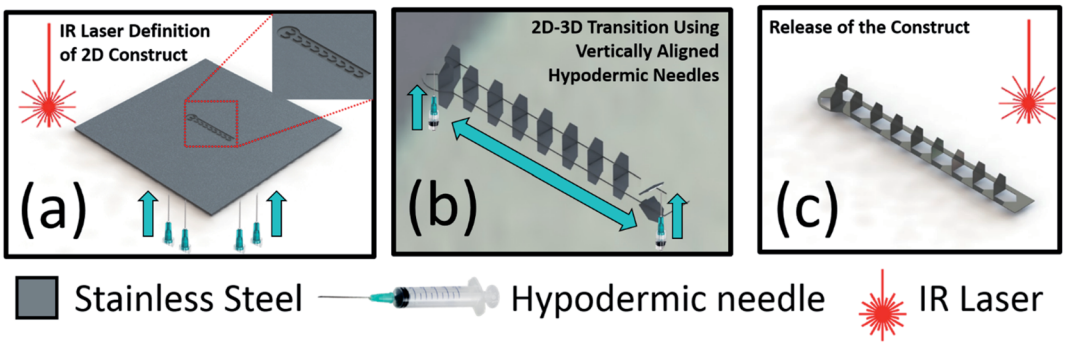


Fig. 1 Schematic process flow for laser micromachining of 3D microneedle electrodes: (a) laser micromachining a obelisk-type geometry using 1064 nm (IR) wavelength using Quick Laze 50ST2, Eolite Lasers onto a stainless steel substrate having a thickness of 25 μm; (b) transitioning the laser micromachined area out-of-plane using a hypodermic needle and releasing the 3D microneedles from the bulk stainless steel substrate by laser micromachining at the same wavelength, 1064 nm (IR); (c) the keyhole of the released 3D microneedles. The microneedle electrodes have a width of 300 μm, height of 400 μm and a pitch of 600 μm. The keyhole cutout in the stainless steel sheet is further obtained shown as inset.

of the laser micromachining of the SS sheet (25 μm thick) micromachined with infrared laser wavelength (1064 nm) using the QuikLaze 50 ST2 laser micromachining system (Eolite Lasers, Portland, OR, USA) with the close-up of the micromachining pattern shown in the inset. The laser was operated at a repetition rate of 50 Hz with a scanning speed of 40 μm $s^{-1}$. The obelisk shaped cut-outs in SS were transitioned out of plane into a 3D configuration using a hypodermic needle [Fig. 1(b)]. Fig. 1(c) shows the schematic of the 3D MEA after it has been released from the SS substrate and the inset shows the cutout in the SS substrate which would be used in subsequent processing steps as a shadow mask to cast silver conductive paste and bond the MEA with the glass chip.

### 2.2 Assembly and packaging of the device

The SS 3D electrodes were assembled on a highly transparent glass chip (22 mm × 22 mm × 0.5 mm) to allow for simultaneous optical and electrical probing [Fig. 2(a)]. The glass substrate was first cleaned in KOH (potassium hydroxide) in IPA (isopropyl alcohol/2 propanol). The IPA allowed for a slowing down the etch rate of glass in KOH along with enabling a smoother surface finish.[27] For electrical probing from the 3D MEA, traces of (Ti; 4N5 purity pellets) and gold (Au; 5N purity pellets) (Kurt J. Lesker, Jefferson Hills, PA, USA) were deposited by electron-beam (E-beam) evaporation (Thermionics Laboratory Inc., Port Townsend, WA, USA) through a shadow mask fabricated out of Kapton®. The shadow mask design had probing pads in place for vias of the 3D printed frame, which was retrofitted on to the glass chip [Section 2.3]. The traces and probing pads for the shadow mask were designed in SolidWorks. The traces are designed to be 150 μm wide and ~7–16 mm long depending upon the position of the electrode and the pad. The dimension of the probing pads was 1 × 1 mm with a pitch of 4 mm. The Kapton® mask was ablated with a QuikLaze 50 ST2 laser micromachining system (Eolite Lasers, Portland, OR, USA) (UV wavelength: 355 nm, scanning speed of 70 μm $s^{-1}$, repetition rate: 50 Hz) [Fig. 2(b)] prior to the metallization [Fig. 2(c)]. Subsequently, the SS keyhole cutout mask [inset of Fig. 1(c)] was placed on top of the glass chip and aligned with the central region of the glass chip [Fig. 2(c)] and the 3D MEA was bonded to the glass substrate with silver

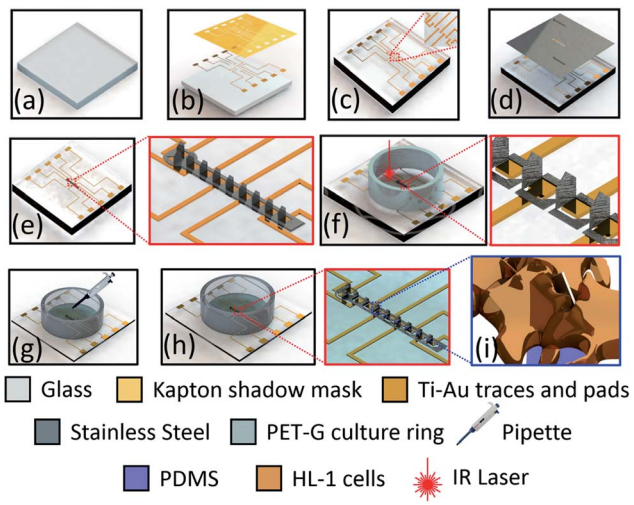


Fig. 2 Schematic process flow of glass chip fabrication and stainless steel assembly: (a) glass chip (500 μm thickness) cleaned in ~2 M solution of KOH (potassium hydroxide) in IPA (isopropyl alcohol; 2-propanol); (b) metallization of a stack of titanium–gold (30 nm–90 nm) using electron beam evaporation through a Kapton shadow mask. The Kapton shadow mask was laser micromachined using 355 nm (UV) using the same Eolite Laser; (c) the titanium–gold traces are 150 μm wide and the contact pads at the periphery of the chip are designed to be 1 mm × 1 mm; (d) the 3D microneedle electrodes are aligned with the metal traces and bonded using silver paste. The silver paste is cast through the SS cutout; (e) the glass chip bonded to the 3D stainless steel keyhole having 10 microneedles using silver paste; (f) a PET-G culture ring is attached using PDMS and the 3D microneedles are isolated from each other using laser micromachining (1064 nm) to yield ten (10) of 3D recording/stimulating electrodes; (g) controlled precision drop-casting and self-planarization of PDMS to achieve the insulation layer; (h) the volume of PDMS controls the height of the PDMS insulation in the area confined by the PET-G ring and determines the geometric area of the 3D Microneedle Electrode Array (MEA); (i) HL-1 cells interacting with a singular 3D microneedle electrode.

conductive paste (PRIMA-SOLDER™ EG8050, AI Technology, Ellsworth Adhesives, Germantown, WI, USA) [Fig. 2(d)]. Curing of the silver paste was performed for a period of 48 hours at 55 °C in an oven. Fig. 2(e) depicts the schematic of the device after the 3D MEA was bonded onto the glass chip with traces. PET-G (polyethylene terephthalate glycol) culture wells having an outer diameter of 16 mm and an inner diameter of 14 mm were bonded with PDMS (poly dimethyl siloxane, chemical formula: $(C_{10}H_8O_4)_n$) to act as a biocompatible adhesive layer [Fig. 2(f)]. The PET-G culture rings were machined from a parent tube (Barrow PET-G tubing, 12 mm ID, 16 mm OD, 500 mm length) using a Horizontal Band Saw (Wellsaw, MI, USA). Both the PET-G culture well and PDMS are biocompatible which makes the MEA chip suitable for biological applications.[11,28]

Individual 3D microelectrodes were isolated from each other using QuikLaze 50 ST2 laser micromachining (IR wavelength: 1064 nm, scanning speed of 40 μm $s^{-1}$, repetition rate: 50 Hz) so that the device is equipped with ten (10) recording/stimulating sites [Fig. 2(f)]. The laser micromachining process was able to ablate all the way through the SS substrate and the underlying silver paste but stop on glass due to the precision ablation capabilities and multimodality of the system which allows for switching between several wavelengths to ablate specific materials. Insulation of the glass chip, metal traces and electrodes to realize the 3D MEA was performed with a PDMS drop-casting step inside the PET-G culture well. Such a controlled precision drop-casting technique [Fig. 2(g)] allows for controlling the size/area of the 3D MEA. The PDMS was cured for 18 hours at 50 °C to realize the final device [Fig. 2(h)]. The schematic, Fig. 2(i) depicts the culturing and interaction of HL-1 cells with a 3D microelectrode.

### 2.3 Integration of custom 3D printed, interconnect packaging frame for interfacing with commercial electronics amplification systems

To interface the fabricated device with commercially available data acquisition systems a custom designed 3D printed interconnect frame with vias and channels was fabricated. SolidWorks was used to design a custom interconnect packaging frame for interfacing with commercial electronics amplification systems (in this case Axion BioSystems MUSE, Axion BioSystems Inc., Atlanta, GA, USA).[29] The packaging frame consists of two parts which slide onto the glass chip on either side as observed in Fig. 3(a). The length of the frame is 24 mm with a width 12 mm and a thickness of 2 mm, all dimensions to be consistent with a modified MUSE system. The frames are designed to have ~510 μm grooves onto which the glass chip of thickness ~500 μm slides seamlessly. Each frame has a total of five vias, whose dimensions were 1 mm in diameter and these vias align on top of the contact pads on the glass chip. The vias transition the contact pads electrically from the top side of the glass chip to the bottom side of the 3D printed frame once the vias and the grooves are filled completely with conductive silver paste [Fig. 3(b)]. The frames were 3D printed on the Asiga MAX UV Digital Light Processing (DLP) system, (Alexandria, NSW, Australia) with high temperature resistant resin (RS-F2-HTAM-02, FormLabs, Sommerville, MA, USA) having a heat deflection temperature (HDT) of 238 °C @ 0.45 MPa. After the material was printed, it was cleaned for 10 minutes in an isopropyl alcohol (IPA) bath and subsequently dried in an oven. The 3D printed frame was finally cured in an UV enclosure (385 nm UV wavelength) of a period of 180 seconds to completely crosslink the resin after printing. The purpose of the vias was to transition the probing pad on the glass substrate to the bottom side using an ink casting step with silver adhesive [Fig. 3(b)].

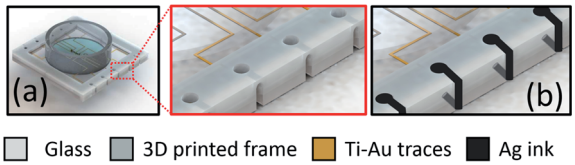


Fig. 3 Schematic process flow of interconnect fabrication: (a) affixing a 3D printed frame printed using Asiga MAX 27UV DLP 3D printer. Two frames slide onto each side of the glass. The frames have a designed groove of 700 μm into which the glass chip slides into. The diameter of the vias is 1 mm and the channel which transitions the vias to the bottom side of the frame is 1 mm wide; (b) silver ink casting of the 3D printed vias effectively transitions the gold pads on the top side of the glass chip to silver pads on the bottom side of the 3D printed frame.

### 2.4 Characterization

Impedance measurements of the 3D MEA were performed using Bode 100 (Omicron Labs, Houston, TX, USA) with Dulbecco's Phosphate Buffer Solution (Thermo Fisher Scientific, Waltham, MA, USA) as the electrolyte. The impedance scans were carried out from 100 Hz to 1 MHz with a platinum wire (eDAQ, Denistone East, Australia) as the counter electrode. Optical imaging of the HL-1 cells was captured using an Eclipse TS2 microscope (Nikon, Japan). Scanning Electron Microscope (SEM) imaging were performed using JSM 6480 (JEOL, Peabody, MA, USA). For imaging conductive samples like stainless steel, the samples were directly loaded onto the chuck of the SEM and imaged using the secondary emission mode. A vacuum level of $10^{-3}$ Pa was maintained, and images were procured at a working distance of ~20 mm at an accelerating voltage between 10–30 kV. For imaging non-conductive surfaces like PDMS insulation, the SEM conditions were kept the same except that the samples were coated with a thin film of gold (~15 nm) to prevent charging while imaging. The resistance of the silver ink filled vias were measured using Keithley 2400 Source meter (Tektronix, Beaverton, OR, USA). The angular distribution of the microelectrodes with respect to the normal were calculated from the SEM images using ImageJ, a public domain Java-based image processing program. The measured impedance was fitted using a MATLAB® code as reported by the authors[24] in which the eqn (1):

$$Z(\omega) = R_S + \left[\frac{1}{C_{DL}(\omega)} + \frac{1}{R_{CT} + W(\omega)}\right] \quad (1)$$

is solved to extract the solution resistance ($R_S$), charge transfer resistance ($R_{CT}$), double-layer capacitance ($C_{DL}$), and the Warburg element ($W$).

### 2.5 Cardiac cell culture

The electrogenic HL-1 cell line was cultured on the microfabricated and assembled 3D MEA to determine the device's ability to capture electrophysiological activity. HL-1 cells are immortalized mouse atrial cardiomyocytes that continuously divide and spontaneously contract in culture, while maintaining a differentiated adult cardiac phenotype.[30] Prior to cell culture, the MEA were sterilized using an isopropyl alcohol wash for 30 minutes. The MEA were subsequently coated with a gelatin/fibronectin extracellular matrix solution and incubated for 12 hours to encourage the cells to adhere to the MEA surface. Cells were initially cultured in cell culture flask (T25 Fisher Scientific) with supplemented Claycomb medium (Sigma-Aldrich, St. Louis, MO; 51800C-500ML) and passaged following a standard procedure when they reached confluency (approximately 48 hours). Cells were then counted using a standard hemocytometer protocol with trypan blue (Gibco, Waltham, MA). Approximately, 31 000 cells were subsequently seeded onto the MEA and incubated at 37 °C with 5% $CO_2$. Supplemented Claycomb cellular media was changed every day. On the 3D MEAs in which the cells reached confluence and began to produce visible beating between 2–4 DIV (days *in vitro*), electrophysiological measurements were performed by interfacing the device with the Axion BioSystems MUSE electrophysiological measurement system after 2 DIV. Spiking activity 6 times above the root mean square (RMS) noise of the system were recorded as action potentials.

## 3. Results and discussions

### 3.1 Microfabrication of three-dimensional stainless steel microneedle electrode array (MEA)

Fig. 4(a) shows the SEM images of the 3D MEA after it has been transitioned out-of-plane using a hypodermic needle. Fig. 4(b) shows a close up SEM image of the 3D MEA. The individual 3D microelectrodes were perpendicular with respect to the horizontal. A box plot of the angular tilt of the 3D MEA is further depicted in Fig. 4(c) emphasizing the consistency of angles of every single microelectrode with respect to the horizontal. For a total of 10 electrodes, the maximum angle of tilt was 90° with a minimum of 86°. An average value of 89° with respect to the horizontal was obtained for the 3D microelectrodes. Such a consistent angle was repeatable across multiple 3D MEAs. Fig. 4(d) depicts an SEM image of the 3D MEA bonded to the glass substrate using silver paste after laser isolation of the ten (10) recording/stimulating sites. Fig. 4(e) shows a close up SEM image depicting the scribe lines of the laser to isolate the microneedles of the electrode array. Fig. 4(f) depicts an SEM image of the completed 3D MEA after controlled precision drop-casting process using PDMS insulation. The CPDC technique yields a PDMS insulation having a thickness of ~250 μm. The CPDC process can further be optimized to realize 3D electrodes of varying sizes as the PDMS casting is performed after affixing the Polyethylene Terephthalate Glycol (PET-G) culture well onto the glass chip which restricts the insulation material (PDMS) within the confines of the culture well. It is observed that the CPDC technique insulates the entire device and exposes the SS tips at a height of ~400 μm to realize the 3D MEA as observed in the inset of Fig. 4(f). SEM images of 3D microelectrodes depicted in figure [Fig. 4(b–d)] represents fabricated device dimensions of 400 μm height, 300 μm width ($N = 10$ in an array) at a pitch of 600 μm which is as per the design dimensions. We have also carried out analysis of the angular tilt of the 3D microelectrodes after the CPDC step to delve into the effect of the insulation strategy on the geometry of the finished device. It is observed that the angular tilt of the 3D microelectrodes remains ~88.1° (Mean of $N = 10$) after CPDC [Fig. 4(g)] which is identical to ~89° (Mean of $N = 10$), which was obtained for the angular tilt of the 3D MEA before CPDC. This finding is attributed to the mechanical stiffness of the SS material and highly favorable method of CPDC. The simple pour-planarize-cure technique does not induce any stress on the 3D MEAs and therefore the angular tilt remains almost constant. Also, the spacing between the tips of the 3D microelectrodes has been plotted for measuring the uniformity across the 3D MEA. It is observed that the spacing between the tips remain extremely close (593 μm [average of $N = 7$] before CPDC and 595.5 μm [average of $N = 7$] after CPDC as depicted in Fig. 4(h) and (i) respectively) to the expected value of the pitch of 600 μm between the electrodes in spite of some microneedles making acute angles with the horizontal. This may be explained as follows: if we assume that a single 3D microelectrode is having another 3D microelectrode on its either side and the flanked 3D microelectrode makes an acute angle with the horizontal, the tip spacing is reduced from the neighboring 3D microelectrode while it is increased with respect to the other neighbor. This causes the mean spacing between the 3D microelectrodes to remain close to the design pitch of 600 μm. Thus, it may be concluded that the CPDC does not interfere with the tip spacing and parallelism of the finished device.

Fig. 5 show the photomicrographs of the device fabrication and assembly in various stages during the realization of the 3D MEA. Fig. 5(a) shows the photomicrograph of the Ti–Au traces as obtained after e-beam evaporation through the laser micromachined Kapton® shadow mask. Fig. 5(b) depicts the photomicrograph of the device after the 3D MEA is bonded to the glass substrate using the silver paste. The 3D MEA is subsequently laser micromachined to isolate individual 3D microelectrodes from each other and insulation of the traces and MEA is achieved using PDMS CPDC inside the PET-G culture well to yield the assembled device [Fig. 5(c)]. Fig. 5(d) details a photomicrograph of the device with the 3D printed frames attached on both sides of the glass chip to realize the final packaged device. Fig. 5(e) portrays a close-up image of the 3D printed frame with the vias which can be subsequently filled with silver paste to transition the gold probing pads on the glass chip to the bottom side of the 3D printed frame with the help of the ink-cast *via* on the outer rim of the 3D printed frame [Fig. 5(f)].

It may be noted here that the microfabrication and assembly process is not only rapid but allows for several other advantages over conventional fabrication of 3D MEAs. A technological summary comparing our approach with some recent

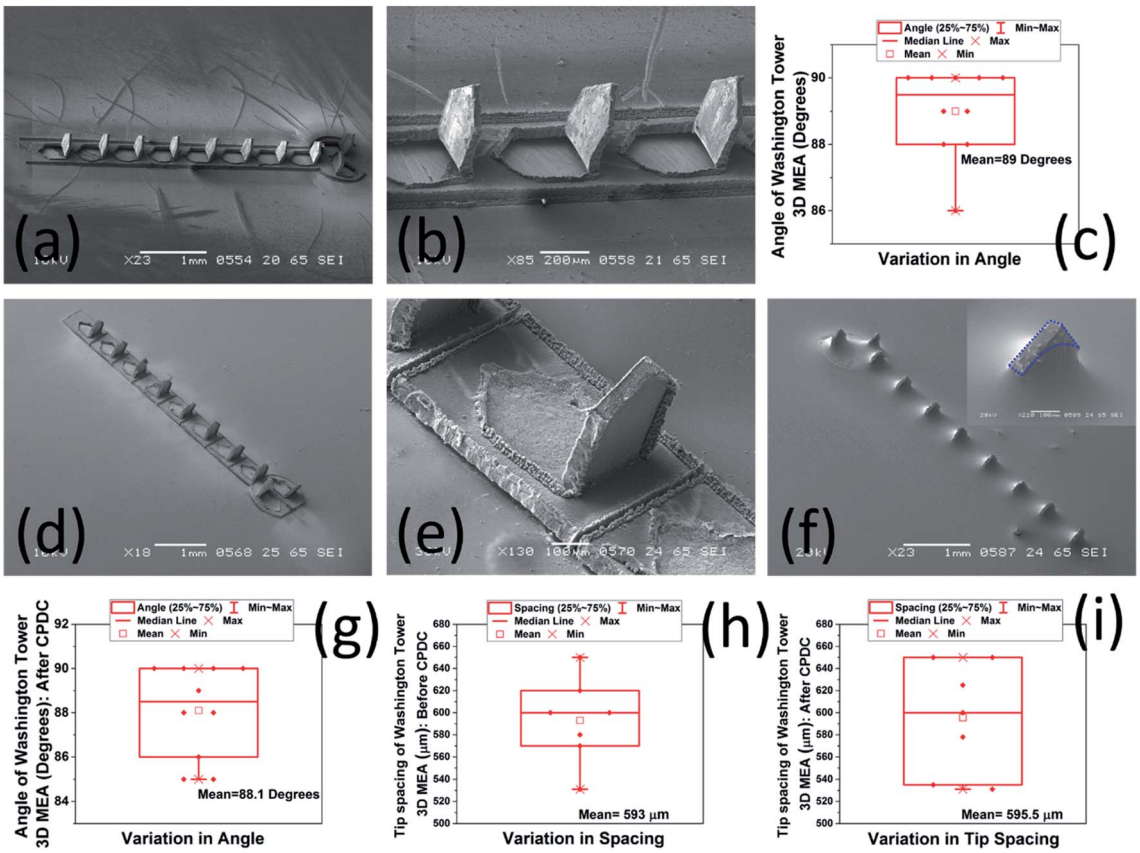


Fig. 4 SEM images of the obelisk-type 3D microneedles after each of the microneedles have been transitioned out-of-plane. The keyhole pattern has not been released from the stainless steel substrate as observed in (a). The close-up SEM images of the 3D microneedles is shown in (b); (c) box plot of the angle of tilt for the 3D microneedles transitioned out-of-plane after laser micromachining ($N = 10$); (d) SEM image of the laser scribed keyhole array to define 10 individual 3D microneedle electrodes. (e) A close-up SEM image shows the laser scribe lines and the 3D microneedle resting on a layer of silver paste; (f) SEM image of the PDMS insulated 3D MEA. PDMS insulates the traces and the planar portions of the device to yield the recording/stimulating sites at a height of ~400 μm. Close-up of a singular 3D microneedle electrode is shown as an inset. (g) Box plot of the angle of tilt for the 3D microelectrodes transitioned out-of-plane after laser micromachining and CPDC ($N = 10$). (h) Box plot of the tip spacing between the 3D microelectrodes transitioned out-of-plane after laser micromachining ($N = 7$). (i) Box plot of the tip spacing between the 3D microelectrodes transitioned out-of-plane after laser micromachining and CPDC ($N = 7$).

technologies[31,32] is conducted in Table 1, where it is observed that laser micromachining and additive manufacturing based makerspace microfabrication approach compares favorably with other approaches in environment, number of process steps, time, cost and equipment/materials.

### 3.2 Electrical characterization

Full spectrum impedance measurements of the 3D MEA were measured in Dulbecco's Phosphate Buffer Solution, (1×, Thermo Fisher Scientific, Waltham, MA, USA). Fig. 6(a) and (b) show the impedance spectra of the 3D MEA after they were assembled (without interconnect frame) and packaged, *i.e.* after attachment of the interconnect frame (average of $N = 3$ electrodes for both combinations). The measured values were fitted with Randles' equivalent circuit model [Fig. 6(c)], a common impedance model used for microelectrodes.[33,34] Both these data sets are very similar depicting minimal change from 3D MEA fabrication on the glass substrate to packaging with the 3D printed frame. The microfabricated 3D MEA having an area of ~0.03 $mm^2$ demonstrates an impedance and phase of ~6.9 kΩ and −12.3° at an electrophysiological relevant frequency of 1 kHz. For the packaged device the real part of the average impedance was 13.3 kΩ with phase of −12.1° at 1 kHz. These values were found to be identical to other reports in literature for similar sized microelectrodes.[11,24,35]

Further, from the extracted parameters [Table 2] it is observed that the 3D printed frame does not affect the performance of the 3D MEA, especially for the values of the double layer capacitance ($C_{DL}$) and $R_s$ which remain unaltered. Changes in charge transfer resistance ($R_{CT}$) and the Warburg element were additionally observed to be within expected limits.[24,36–38] This was attributed to the low DC resistance of the silver ink casted vias in the 3D printed frame. Fig. 6(d) portrays a box plot of the measured resistance of vias ($N = 10$). The mean resistance of this set of vias was 3.99 Ω. The differences in results were less than ±1.00 Ω when compared to the mean. This value was found to be similar across multiple devices.

 

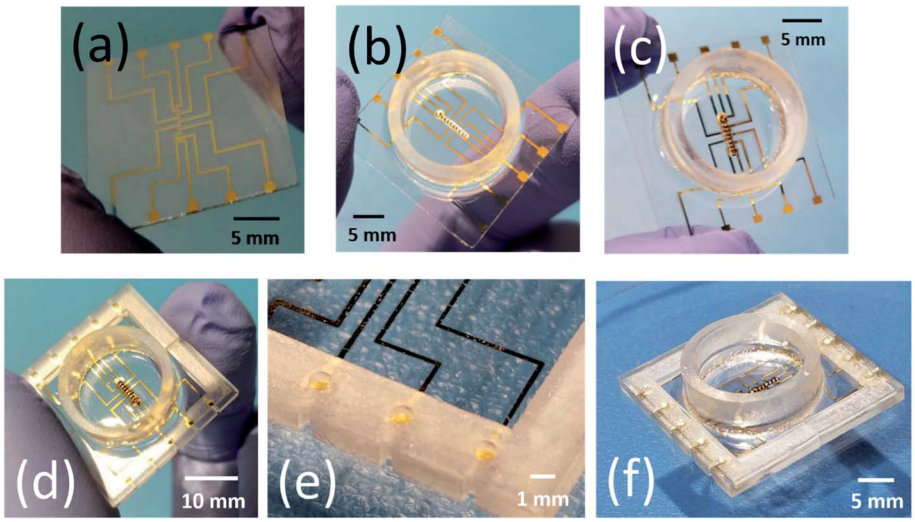


Fig. 5 Optical photomicrographs of the fully assembled device: (a) glass chip with Ti–Au metal traces and pads; (b) photomicrograph of the device after the 3D microneedles are bonded to the glass substrate using silver paste and subsequently laser micromachined to be isolated from each other as depicted in (c); (d) fully assembled device with the 3D printed frame slid onto the glass chip; (e) close up image of the 3D printed *via* showing the metallized gold pad aligned with the vias on the 3D printed frame; (f) ready-to-interface device with the vias filled with silver paste so that the gold traces on the top side of the glass chip transitions to the bottom side of the packaged device.

Table 1 Technological summary of the microfabrication development between makerspace microfabrication and other recent approaches[31,32]

| | Glass/silicon-based microfabrication | This work: makerspace microfabrication |
|---|---|---|
| Environment | Cleanroom | Makerspace/Benchtop |
| Process steps | 12 for 3D probe fabrication, 4 for actuation shank design and fabrication[31]<br>10 for 3D gold mushroom shaped electrodes[32] | 8 for 3D MEA fabrication, 2 for packaging |
| Resolution | <1 μm | ~1 μm (subtractive)/27 μm (additive) |
| Total time | Up to 16 weeks | ~2 weeks |
| Cost | $$$$ | $ |
| Fabrication equipment | Mask aligner, fumehood, spinner, hot plate, wire-bonder, die attach, E-beam evaporator, mask maker/high res. printer, dicing saw, *etc.* | 3D printer, oven, UV-lamp, micromill, laser, spinner, benchtop sputterer or E-beam evaporator |
| Packaging equipment | PCBs requiring design and external packaging fabrication | 3D printed jigs and fixtures |
| Materials | Glass wafer, photoresist, photo mask, isopropanol, metal pellets/metal target, insulation, electroplating materials solvents, PCB, gold wire, *etc.* | Glass wafer, SS sheets, 3D printing resin, isopropanol, stencil mask, conductive ink, insulation |
| Electrodes | 80 per array[31] | Up to 64 (not depicted in this work but scalable to 64) |
| Customization | Limited by cleanroom and mask used for photolithography | Rapid customization possible with on-the-fly design changes |

### 3.3 3D MEA noise measurement and electrophysiological signatures with HL-1 cells

Fig. 7 shows the fabricated device interfaced with the Axion BioSystems MUSE electronics amplifier [Fig. 7(a) and (b)]. The design was intended for intimate connectivity between the device and the amplifier system, and the results clearly illustrate the accomplishment of this goal. Fig. 7(c) depicts peak to peak noise measured from the device and its connectivity to the MUSE system. This signature was post processed in MATLAB from raw data collected using Axion BioSystems AxIS software (Axion BioSystems Inc., Atlanta, GA, USA). The peak to peak noise of the 3D MEA is observed to be ideal for neural and cardiac signal acquisition. The average RMS noise across multiple microelectrodes was observed to be ~4.2 μV.

Recent literature provides a comparison for not only the relevancy of this approach, but its comparative performance to similar 2D and 3D MEAs that were evaluated using the same HL-1 cell line. As an example, Garma *et al.*[39] report a complete 2D MEA recording platform (costing ~6000€ for the system and the MEAs), that interfaces to the commercial Multichannel

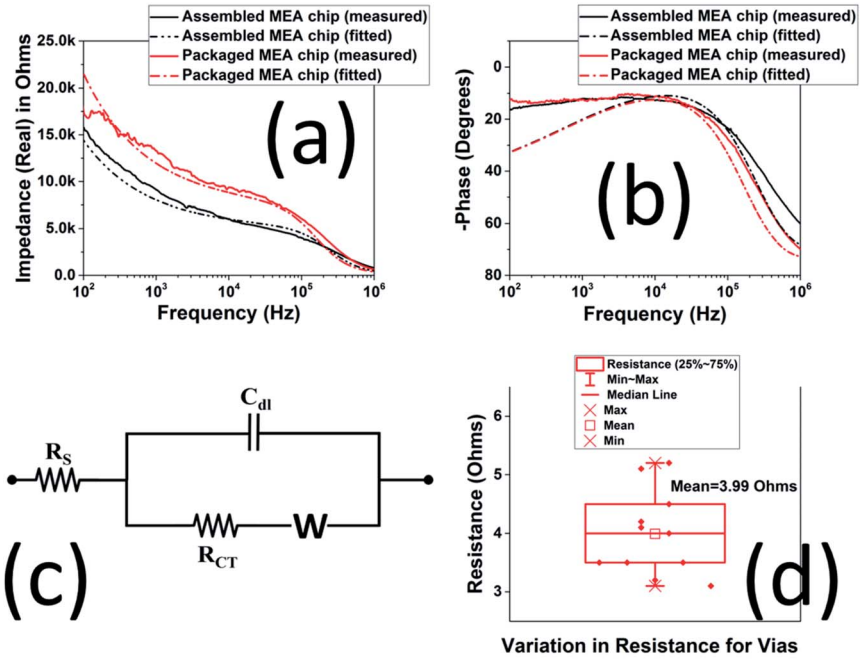


Fig. 6 (a) Impedance (real) spectra of the assembled device, packaged device with 3D printed frame and fitted plot as per Randles equivalent circuit; (b) phase spectra of the assembled device, packaged device with 3D printed frame and fitted plot as per (c) Randles' equivalent circuit used for circuit fitting and extraction; (d) box plot of the DC resistance of the vias after silver ink casting process.

Table 2 Extracted parameters from the fitted model as per Randles' equivalent circuit

| 3D MEA | $R_s$ (Ω) | $R_{CT}$ (kΩ) | $C_{dl}$ (nF) | $W$ ($\times 10^5$) (1/Ω $s^{-0.5}$) |
|---|---|---|---|---|
| Assembled MEA chip | 181 | 5.0 | 0.125 | 3.25 |
| Packaged MEA chip | 181 | 7.5 | 0.125 | 4.875 |

Systems (MCS) GMBH 64-electrode system. The average 1 kHz impedance of this system was reported as 160.06 kΩ, with an estimated RMS noise of ~20–25 μV. In comparison to such 2D MEAs, we have successfully demonstrated MEAs with 3D functionality with an order of magnitude better impedance and noise characteristics. We expect our devices to depict improved signal-acquisition abilities, and higher device sensitivity imparted by the lower impedance microelectrodes which are able to innervate deeper into the cell culture.

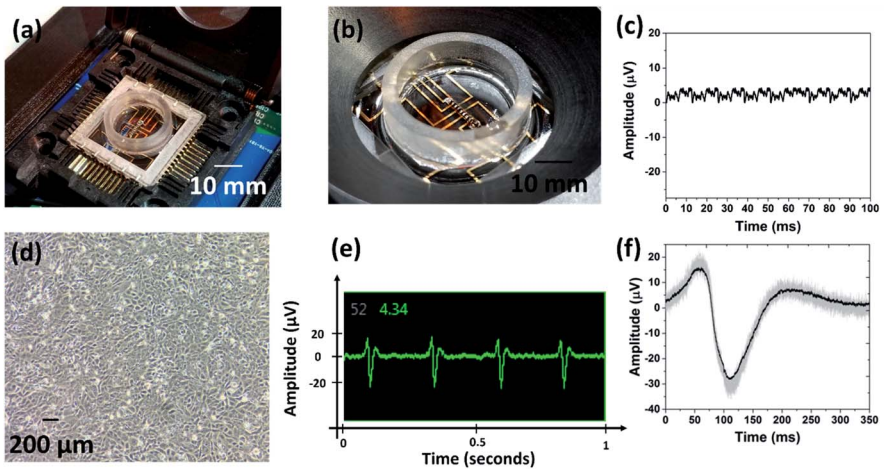


Fig. 7 (a) and (b) The packaged device connected to the commercial Axion BioSystems MUSE electronics interface; (c) representative noise plot of one of the microelectrodes of the 3D MEA; (d) optical photomicrograph of HL-1 cells after 2 DIV; (e) screen capture of cardiac beats from AxIS software from a single 3D microneedle electrode; (f) post processed, exaggerated plot of a repeatable single beats from HL-1 cells cultured on the 3D MEA.

 

Fig. 7(d) portrays optical photomicrograph of the HL-1 cell line at 2 days *in vitro* (DIV). This image was captured using transmitted light microscopy in a culture flask where the cells are grown prior to transfer into the 3D MEA. Fig. 7(e) is a cropped screen capture of an active recording channels in Axion BioSystems AxIS recordings software, showing extracellular action potentials of HL-1 cells. The cells were beating spontaneously at approximately 5 Hz on the 3D MEA device and produced typical cardiac action potentials of approximately 40 μV peak-to-peak. Fig. 7(f) shows a superposition of 25 cardiac action potentials (average of all 25 signals is highlighted). The beating activity demonstrates the device's functional biocompatibility, good electrophysiological interfacing, and biosensing capabilities, as cells were able to proliferate and beyond that were able to produce the molecular machinery required to produce action potentials as well as contractions.

## 4. Conclusions

In this paper, the microfabrication and assembly of 3D stainless steel microneedle electrode array (3D MEA) on a glass substrate for simultaneous optical and electrical probing of electrogenic cells has been reported. The developed makerspace microfabrication technology involved laser micromachining, e-beam metallization, 3D printing, ink casting, PDMS insulation with materials having biological compatibility to adapt it as a tool for interrogation of 3D cell culture models. The orientation of the 3D microelectrodes ($N = 10$) measures an average of 89° with the horizontal and was found to be consistent across multiple devices. Electrical impedance spectroscopy of the fully fabricated and assembled device produced a real impedance of 6.9 kΩ with phase of −12.3°@1 kHz (for the fabricated device) and 13.3 kΩ with phase of −12.1°@1 kHz (for the assembled device). Both of these values are comparable to other reported values in literature. The packaged interconnect vias additionally measured 3.99 Ω (for $N = 10$ vias). The 3D MEA was further interfaced with commercial electronics amplification system and reported electrodes with an excellent RMS noise of 4.2 μV.

The 3D MEA fabrication presented here demonstrates an order of magnitude lower performance for both RMS noise and microelectrode impedance to that of a comparable 2D MEA characterized using the spontaneous beat activity of HL-1 cells.[39] Our platform illustrates how a relatively simple fabrication strategy, through makerspace microfabrication, can result in a complex and nuanced 3D MEA in less time, and at a significantly lower cost. As a comparison, the 3D MEA produced by Brüggemann *et al.*[40] requires a complex lithography fabrication approach, which, while advanced in its own right, presents an opportunity cost which may be too high for low resource settings and universities/commercial entities without extensive facilities.

Lastly cardiac beats were recorded from an immortal mouse cardiac cell line (HL-1) at 2 DIV depicting an end to end design, fabrication, packaging and characterization of the device. Such a device is expected to play a vital role in the burgeoning and rapidly growing "Organ-on-a-Chip" field. Further this device represents a cost effective, rapidly fabricated biosensing platform for medical and pharmaceutical research.

## Conflicts of interest

Prof. Rajaraman is a co-founder and equity stake holder in Axion BioSystems Inc. Additionally, Prof. Rajaraman and Dr Sommerhage have a potential competing financial interest, namely a company being formed that potentially could market services for the methods described herein. Both will have financial interests when the company is incorporated. The other authors have no conflicts of interest to report.

## Acknowledgements

Paola M. Morales-Carvajal (Biomedical Engineering Department, Polytechnic University of Puerto Rico, San Juan, PR 00918) would like to thank the National Science Foundation for support of this work through REU site EEC 1560007 and members of the NanoBioSensors & Systems Laboratory, staff and faculty members of NanoScience Technology Center (NSTC) for all the support and guidance through this journey. Additionally, we would like to thank the University of Central Florida (Orlando, FL, USA) start-up funding of Prof. Rajaraman for partially funding this work and the Materials Characterization Facility (MCF). This effort was also partially funded through NIH NIEHS SBIR sub-contract R43ES029886-01 and NSF I/UCRC funding through the MIST Center (http://www.mist-center.org).

## References

1 H. Lodish, A. Berk, S. L. Zipursky, P. Matsudaira, D. Baltimore and J. Darnell, *Molecular cell biology*, National Center for Biotechnology Information, Bookshelf, 4th edn, 2000.
2 G. G. Matthews, *Cellular physiology of nerve and muscle*, Wiley Online Library, 2003.
3 S. Jeong, S. Kim, J. Buonocore, J. Park, C. J. Welsh, J. Li and A. Han, A three-dimensional arrayed microfluidic blood–brain barrier model with integrated electrical sensor array, *IEEE Trans. Biomed. Eng.*, 2017, **65**(2), 431–439.
4 N. Mustapha, J. Prado, C. Margo and A. Rouane, in *Bioimpedance spectroscopy of human blood at low frequency using coplanar microelectrodes, 11th Mediterranean Conference on Medical and Biomedical Engineering and Computing 2007*, Springer, 2007, pp. 186–189.
5 G. Kim, K. Kim, E. Lee, T. An, W. Choi, G. Lim and J. Shin, Recent Progress on Microelectrodes in Neural Interfaces, *Materials*, 2018, **11**(10), 1995.
6 V. Viswam, M. E. J. Obien, F. Franke, U. Frey and A. R. Hierlemann, Optimal electrode size for multi-scale extracellular-potential recording from neuronal assemblies, *Front. Neurosci.*, 2019, **13**, 385.
7 N. Azim, C. Hart, F. Sommerhage, M. Aubin, J. J. Hickman and S. Rajaraman, Precision Plating of Human Electrogenic Cells on Microelectrodes Enhanced With Precision Electrodeposited Nano-Porous Platinum for Cell-

Based Biosensing Applications, *J. Microelectromech. Syst.*, 2019, **28**(1), 50–62.

8 J. H. Hong, J. H. Choi, T. Y. Kim and K. J. Lee, Spiral reentry waves in confluent layer of HL-1 cardiomyocyte cell lines, *Biochem. Biophys. Res. Commun.*, 2008, **377**(4), 1269–1273.

9 P. Wijdenes, H. Ali, R. Armstrong, W. Zaidi, C. Dalton and N. I. Syed, A novel bio-mimicking, planar nano-edge microelectrode enables enhanced long-term neural recording, *Sci. Rep.*, 2016, **6**, 34553.

10 F. M. Watt and W. T. Huck, Role of the extracellular matrix in regulating stem cell fate, *Nat. Rev. Mol. Cell Biol.*, 2013, **14**(8), 467.

11 N. Azim, A. Kundu, M. Royse, Y. Y. L. Sip, M. Young, S. Santra, L. Zhai and S. Rajaraman, Fabrication and Characterization of a 3D Printed, MicroElectrodes Platform With Functionalized Electrospun Nano-Scaffolds and Spin Coated 3D Insulation Towards Multi-Functional Biosystems, *J. Microelectromech. Syst.*, 2019, **28**(4), 606–618.

12 D. Huh, G. A. Hamilton and D. E. Ingber, From 3D cell culture to organs-on-chips, *Trends Cell Biol.*, 2011, **21**(12), 745–754.

13 J. W. Haycock, 3D cell culture: a review of current approaches and techniques, in *3D cell culture*, Springer, 2011, pp. 1–15.

14 R. M. Huval, O. H. Miller, J. L. Curley, Y. Fan, B. J. Hall and M. J. Moore, Microengineered peripheral nerve-on-a-chip for preclinical physiological testing, *Lab Chip*, 2015, **15**(10), 2221–2232.

15 S. N. Bhatia and D. E. Ingber, Microfluidic organs-on-chips, *Nat. Biotechnol.*, 2014, **32**(8), 760.

16 Z. Koledova, *3D Cell Culture: Methods and Protocols*, Springer, 2017.

17 D. Bušek and P. Mach, in *Study of glass transition temperature of electrically conductive adhesives, 2012 IEEE 18th International Symposium for Design and Technology in Electronic Packaging (SIITME)*, IEEE, 2012, pp. 143–146.

18 A. D. Sharma, L. McCoy, E. Jacobs, H. Willey, J. Q. Behn, H. Nguyen, B. Bolon, J. L. Curley and M. J. Moore, Engineering a 3D functional human peripheral nerve *in vitro* using the Nerve-on-a-Chip platform, *Sci. Rep.*, 2019, **9**(1), 8921.

19 U. Egert and T. Meyer, Heart on a chip—extracellular multielectrode recordings from cardiac myocytes *in vitro*, in *Practical methods in cardiovascular research*, Springer, 2005, pp. 432–453.

20 B. Ghane-Motlagh and M. Sawan, in *A review of microelectrode array technologies: design and implementation challenges, 2013 2nd International Conference on Advances in Biomedical Engineering*, IEEE, 2013, pp. 38–41.

21 R. Kim, S. Joo, H. Jung, N. Hong and Y. Nam, Recent trends in microelectrode array technology for *in vitro* neural interface platform, *Biomed. Eng. Lett.*, 2014, **4**(2), 129–141.

22 Z. Aqrawe, J. Montgomery, J. Travas-Sejdic and D. Svirskis, Conducting polymers for neuronal microelectrode array recording and stimulation, *Sens. Actuators, B*, 2018, **257**, 753–765.

23 R. Wang, X. Huang, G. Liu, W. Wang, F. Dong and Z. Li, Fabrication and characterization of a parylene-based three-dimensional microelectrode array for use in retinal prosthesis, *J. Microelectromech. Syst.*, 2010, **19**(2), 367–374.

24 A. Kundu, C. Nattoo, S. Fremgen, S. Springer, T. Ausaf and S. Rajaraman, Optimization of makerspace microfabrication techniques and materials for the realization of planar, 3D printed microelectrode arrays in under four days, *RSC Adv.*, 2019, **9**(16), 8949–8963.

25 A. Kundu, T. Ausaf and S. Rajaraman, 3D Printing, Ink Casting and Micromachined Lamination (3D PICLμM): A Makerspace Approach to the Fabrication of Biological Microdevices, *Micromachines*, 2018, **9**(2), 85.

26 M. O. Heuschkel, M. Fejtl, M. Raggenbass, D. Bertrand and P. Renaud, A three-dimensional multi-electrode array for multi-site stimulation and recording in acute brain slices, *J. Neurosci. Methods*, 2002, **114**(2), 135–148.

27 K. P. Rola and I. Zubel, Impact of alcohol additives concentration on etch rate and surface morphology 28. of (100) and (110) Si substrates etched in KOH solutions, *Microsyst. Technol.*, 2013, **19**(4), 635–643.

28 C. Lacroix, M. Bousmina, P. Carreau, B. Favis and A. Michel, Properties of PETG/EVA blends: 1. Viscoelastic, morphological and interfacial properties, *Polymer*, 1996, **37**(14), 2939–2947.

29 https://www.axionbiosystems.com.

30 W. C. Claycomb, N. A. Lanson, B. S. Stallworth, D. B. Egeland, J. B. Delcarpio, A. Bahinski and N. J. Izzo, HL-1 cells: a cardiac muscle cell line that contracts and retains phenotypic characteristics of the adult cardiomyocyte, *Proc. Natl. Acad. Sci. U. S. A.*, 1998, **95**(6), 2979–2984.

31 D. A. Soscia, D. Lam, A. C. Tooker, H. A. Enright, M. Triplett, P. Karande, S. K. Peters, A. P. Sales, E. K. Wheeler and N. O. Fischer, A flexible 3-dimensional microelectrode array for *in vitro* brain models, *Lab Chip*, 2020, **20**(5), 901–911.

32 S. M. Ojovan, N. Rabieh, N. Shmoel, H. Erez, E. Maydan, A. Cohen and M. E. Spira, A feasibility study of multi-site, intracellular recordings from mammalian neurons by extracellular gold mushroom-shaped microelectrodes, *Sci. Rep.*, 2015, **5**(1), 1–14.

33 D. A. Harrington and P. Van Den Driessche, Mechanism and equivalent circuits in electrochemical impedance spectroscopy, *Electrochim. Acta*, 2011, **56**(23), 8005–8013.

34 G. Brug, A. Van Den Eeden, M. Sluyters-Rehbach and J. Sluyters, The analysis of electrode impedances complicated by the presence of a constant phase element, *J. Electroanal. Chem. Interfacial Electrochem.*, 1984, **176**(1–2), 275–295.

35 G. S. Guvanasen, L. Guo, R. J. Aguilar, A. L. Cheek, C. S. Shafor, S. Rajaraman, T. R. Nichols and S. P. DeWeerth, A stretchable microneedle electrode array for stimulating and measuring intramuscular electromyographic activity, *IEEE Trans. Neural Syst. Rehabil. Eng.*, 2016, **25**(9), 1440–1452.

 

36 C. Karnati, R. Aguilar, C. Arrowood, J. Ross and S. Rajaraman, Micromachining on and of transparent polymers for patterning electrodes and growing electrically active cells for biosensor applications, *Micromachines*, 2017, **8**(8), 250.

37 D. Borkholder, J. Bao, N. Maluf, E. Perl and G. Kovacs, Microelectrode arrays for stimulation of neural slice preparations, *J. Neurosci. Methods*, 1997, **77**(1), 61–66.

38 D. Borkholder, *Cell based biosensors using microelectrodes*, Stanford University, 1998.

39 L. D. Garma, L. Matino, G. Melle, F. Moia, F. De Angelis, F. Santoro and M. Dipalo, Cost-effective and multifunctional acquisition system for *in vitro* electrophysiological investigations with multi-electrode arrays, *PloS One*, 2019, **14**(3), 1–13.

40 D. Brüggemann, B. Wolfrum, V. Maybeck, Y. Mourzina, M. Jansen and A. Offenhäusser, Nanostructured gold microelectrodes for extracellular recording from electrogenic cells, *Nanotechnology*, 2011, **22**(26), 265104.